Commissioning the Texas A&M University Penning Trap via Offline Mass Measurements

Morgan Nasser
nassermorgan@tamu.edu
Cyclotron Institute, Texas A&M University, College Station, TX 77840

July 9, 2020

Abstract

The Texas A&M Penning Trap (TAMUTRAP) facility has been developed in order to probe the symmetries of the charged electroweak sector of the standard model through the observation of $0^+ \rightarrow 0^+$ superallowed transitions in β-delayed proton decay. This will be done using the world's largest cylindrical Penning trap, capable of 4π detection of ≤ 4.75 MeV β-delayed protons from short-lived, neutron-deficient nuclei. This report describes the system, details on how we manipulate the ion motion, and the commissioning work performed which demonstrates the facility's ability to perform mass measurements on stable ions to < 5 parts in 10^8.

1 Introduction

This thesis describes the commissioning of the TAMUTRAP facility via mass measurements of stable ions. This is not part of the overall goal of TAMUTRAP, however it has been performed first for a number of reasons: we have designed a unique Penning trap [1] which we had to demonstrate works like typical cylindrical Penning traps; in order to reduce sources of systematic uncertainty in the β-decay program, we need to excite the ion eigenmotion just like one does for mass measurements; transporting stable ions throughout our beamline allowed us to develop the control systems and optimize the efficiency of the facility.

The long-term goal and global features of TAMUTRAP are outlined below. Following this, we describe how we manipulate ion motions in the trap and techniques used to perform mass measurements. Finally we present the results which demonstrate the efficacy of our novel trap and ability to measure masses to a few parts in 10^8.

1.1 Scientific goals of TAMUTRAP

Fundamental symmetries of the electroweak interaction as described by the standard model (SM) of particle physics have been probed for decades through measurements of nuclear β-decay correlations and comparative half-lives. TAMUTRAP was specifically designed to add to these studies by measuring the correlation between the β and neutrino in a number of β-delayed proton decaying nuclei: ^{20,21}Mg, ^{24,25}Si, ^{28,29}S, ^{32,33}Ar, and ^{36,37}Ca.

In the standard model, the weak nuclear force is a purely vector-minus-axial-vector interaction. However, new models of BSM physics invariably predict contributions from other forms, such as scalar and tensor interactions, which are suppressed relative to the dominant $V - A$ interaction. These novel interactions would affect the correlations between the progeny of β decays. Jackson, Treiman and

Wyld [2, 3] expressed the general decay rate of allowed β decay consistent with Lorentz invariance in terms of coupling constants, C_i, C_i', where $i = S$ (scalar), V (vector), A (axial-vector), T (tensor) and P (pseudo-scalar). Considering $0^+ \to 0^+$ pure Fermi transitions for simplicity (no nuclear polarization or alignment), the decay rate is:

$$\frac{d^5W}{dE_\beta d\Omega_\beta d\Omega_\nu} = \frac{G_F^2}{(2\pi)^5}|V_{ud}|^2 p_\beta E_\beta (A_0 - E_\beta)^2 \left[1 + a_{\beta\nu}\left(\frac{p_\beta}{E_\beta}\right)\cos\theta_{\beta\nu} + b_{\text{Fierz}}\frac{m_e}{E_\beta}\right], \tag{1}$$

where p_β, E_β are the momenta and total energy of the β, $\theta_{\beta\nu}$ is the angle between the β and ν, and the values of the correlation parameters, $a_{\beta\nu}$ and b_{Fierz}, depend on the symmetry-structure of the weak interaction according to

$$a_{\beta\nu} = \frac{|C_V|^2 + |C_V'|^2 - |C_S|^2 - |C_S'|^2}{|C_V|^2 + |C_V'|^2 + |C_S|^2 + |C_S'|^2} \tag{2}$$

$$b_{\text{Fierz}} = -2\sqrt{1-\alpha^2 Z^2}\left(\frac{\text{Re}(C_S C_V^* + C_S' C_V'^*)}{|C_V|^2 + |C_V'|^2 + |C_S|^2 + |C_S'|^2}\right) \tag{3}$$

In the SM, $C_V = C_V'$ and $C_A = C_A'$ with all other couplings zero; this leads to $a_{\beta\nu} = 1$ and $b_{\text{Fierz}} = 0$. If instead scalar and/or tensor interactions exist ($C_S, C_T \neq 0$), then $a_{\beta\nu} < 1$ and $b_{\text{Fierz}} \neq 0$. Measurements of these correlations, particularly b_{Fierz} which is *linear* in the BSM couplings, to $\lesssim 0.1\%$ search for such new physics in a manner complementary to other searches.

In practice, what is actually measured is $\tilde{a}_{\beta\nu}$:

$$\tilde{a}_{\beta\nu} \equiv a_{\beta\nu}\left[1 + b_{\text{Fierz}}\frac{m_e}{\langle E_\beta\rangle}\right]^{-1} \tag{4}$$

where $\langle E_\beta\rangle$ is the β energy averaged over the observed spectrum. In the SM, $\tilde{a}_{\beta\nu}$ is also unity, and the sensitivity to BSM physics goes like:

$$1 - \tilde{a}_{\beta\nu} = 2C_S\frac{m_e}{\langle E_\beta\rangle}\sqrt{1-\alpha^2Z^2} + \mathcal{O}(C_S^2) \tag{5}$$

The value of $\tilde{a}_{\beta\nu}$ will be inferred from measuring the β-delayed proton which inherits information from the β decay through kinematics. Specifically, the Doppler shifts induced by parallel and anti-parallel β decays (i.e. the β and neutrino going same/opposite directions) that propagate into the proton energy spectra are measured. This shift is sensitive to the value of the correlation parameters and thus serves as a probe for high-precision BSM experimentation.

1.2 The TAMUTRAP Facility

Most modern correlation parameter experiments involve confining isotopes in an open geometry using neutral atom or ion traps. One drawback of neutral atom traps is the fact that only certain atoms (alkalis and metastable noble gases, and a few other special cases) have suitable laser transitions for trapping. Ion traps, however, are able to confine any charged particles (e.g. ions) of any element.

A Penning trap confines charged particles to a small, well-defined point in space using a static electric potential well (azimuthal confinement) and a strong linear magnetic field (radial confinement via the Lorentz force). Typically, the homogeneous $B = 4 - 7$ T fields are produced by a superconducting solenoid, and the electric field on the order of 10 V is generated by electrodes using either a hyperbolic or cylindrical geometry. As the sketch of Fig. 1 shows, the much more open geometry of the cylindrical configuration is amenable to observing the progeny of β decay; the hyperbolic configuration is generally

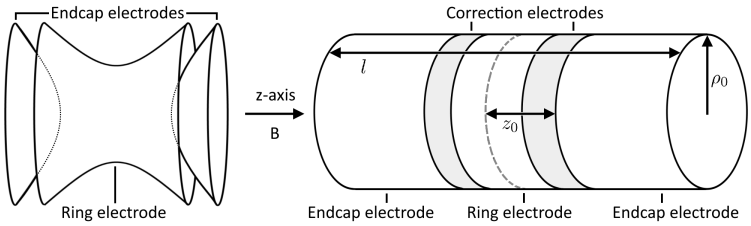

Figure 1: A sketch showing the difference between the two types of Penning traps. A quadrupole electric field is established by the electrode geometry in a hyperbolic trap (left). The same field may be generated in the cylindrical trap of total length l (right) with a proper choice of the ratio of characteristic lengths, ρ_0/z_0, and electrode voltages (ρ_0 is the radius, and z_0 is the length from the trap center to the end of the correction electrode). In both types of trap, a uniform magnetic field runs along the z-axis, which is perpendicular to the plane of symmetry.

used for precision mass measurements. Precision β-decay experiments are well-served by a cylindrical geometry due to the fact that the magnetic field employed to trap the ions radially may simultaneously be used to contain and direct charged decay products [4], such as βs and protons, towards detectors at both ends of the trap with up to 4π acceptance. The electrostatic axial confinement is orders of magnitude weaker than the energy of the decay products, and thus distortions to their momenta are negligible. It is for these reasons that TAMUTRAP has chosen to utilize the cylindrical Penning trap for its decay studies. In addition, this Penning trap may be used for other physics research, including mass measurements, proton decays for nuclear astrophysics and structure, and can provide ultra-pure beams for a general decay station.

Figure 2 shows a CAD drawing of the TAMUTRAP facility, with the major components labelled. Two alkali-ion source stations which provide beams of stable $^{23}\mathrm{Na}^{+}$, $^{39}\mathrm{K}^{+}$, $^{85,87}\mathrm{Rb}^{+}$ and $^{133}\mathrm{Cs}^{+}$ were used to commission and develop the system. The ions are electrostatically directed into the radio-frequency quadrupole (RFQ) Paul trap [5] where they are cooled and bunched, converting the high-emittance continuous beam from the ion source into a tight, pulsed beam of ions. This is necessary for efficient loading in the Penning trap which is installed at the center of the 7T210ASR superconducting solenoid [1, 6, 7].

In order to radially confine all the ≤ 4.75 MeV protons from the β decay of the nuclei of interest to the TAMUTRAP in the 7-T field of our magnet, we require the inner diameter of our trap to be 180 mm. Cylindrical Penning traps already in use [8] have open ends with a length-to-radius ratio of $l/\rho_0 = 11.75$, which is not a viable geometry: a radius of 90 mm would make the length over a meter long, which is longer than the length of the magnet. Thus we developed a new design based on a closed-endcap geometry with $l/\rho_0 = 3.72$ [1] that is only 33.5 cm long. This design not only fits in the solenoid, but also allows us to place biased Si detectors on each end of the trap to detect the βs and protons with 4π acceptance.

2 Manipulation of Ion Eigenmotion in the Trap

The well-defined motion of ions in a trap may be manipulated by exciting one or more of the eigenmotions with rf fields. This is typically done to cool and purify ions, and to perform precision mass measurements. At TAMUTRAP, our focus is not on mass measurements, but we *do* need to be able to manipulate the ion motion in order not to lose events: the end-cap electrodes/detectors must necessarily have small (~ 4-mm diameter) holes for injecting and ejecting the ions which, if the decay occurs on the trap axis, the βs will escape through and not be detected. By exciting their magnetron motion to larger a ρ_- radius, the βs will not exit through the central hole of the detector and we will retain 4π collection of all progeny from the β decays being studied.

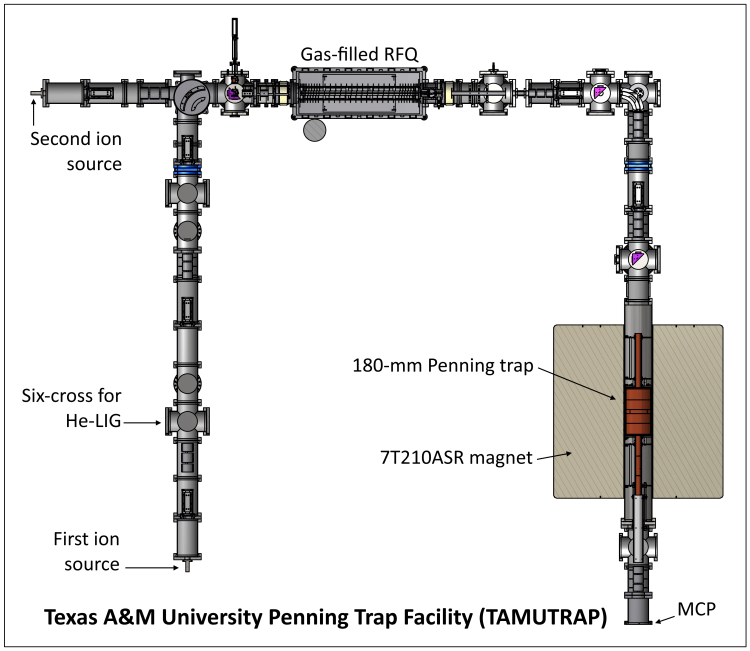

Figure 2: Two alkali sources provide ions which have been used to commission the TAMUTRAP beamline and new trap. The 10-keV ions are guided with x-y steerers and deflectors, and focused with Einzel lenses before entering the RFQ. The RFQ cools and bunches the ions for injection into the Penning trap where we manipulate their eigenmotion and perform mass measurements. Radioactive ion beams from the He-LIG will be brought up from Cave 2 (into the page) and enter the TAMUTRAP beamline via a spherical deflector installed in front of the 1st ion source.

2.1 Ion Motion in a Penning Trap

The defining feature of the Penning trap is its quadratic potential throughout the trapping volume near the center of the trap:

$$V(z,\rho) = \frac{V_0}{d^2(z^2 - \frac{1}{2}\rho^2)}, \tag{6}$$

where $d^2 = \frac{1}{2}(z_0^2 + \frac{1}{2}\rho_0^2)$ is the characteristic length scale, V_0 is the trapping potential and the lengths z_0 and ρ_0 are defined in Fig. 1. The TAMUTRAP geometry has $z_0 = 87$ mm and $\rho_0 = 90$ mm, giving $d = 76$ mm. The potential of Eq. (6) causes an ion to exhibit harmonic motion along the z-axis, but it does not confine them radially; to trap an ion in 3D, a uniform magnetic field is applied along the z-axis, causing the ion to Larmor precess around the trap axis. The combined electric and magnetic fields lead to three eigenmotions: an axial harmonic motion, a planar (reduced) cyclotron orbit, and a planar magnetron orbit. The frequencies of these motions are referred to as ω_z, ω_+, and ω_- respectively[1]. Figure 3 indicates ion trajectories in a Penning trap due to these three eigenmotions.

Figure 4 shows both the concept of our novel Penning trap and the physically constructed one. The electrodes are floated to specific voltages (see Ref. [1] for details) to achieve the quadratic electric field lines shown. The central "ring" electrode is segmented into four pieces allowing for dipolar and quadrupolar excitation via rf-alternating voltages (see Fig. 5 for the configurations). Dipole excitation is performed by alternating opposing segments and produces a kicking action that excites the magnetron motion and radially shifts the ions outwards. As explained earlier, increasing the magnetron radius by such a dipolar excitation is important for TAMUTRAP's β-decay program. Quadrupole excitation

[1]Throughout this report, subscript labels of $+$ and $-$ refer to reduced cyclotron and magnetron motions, respectively.

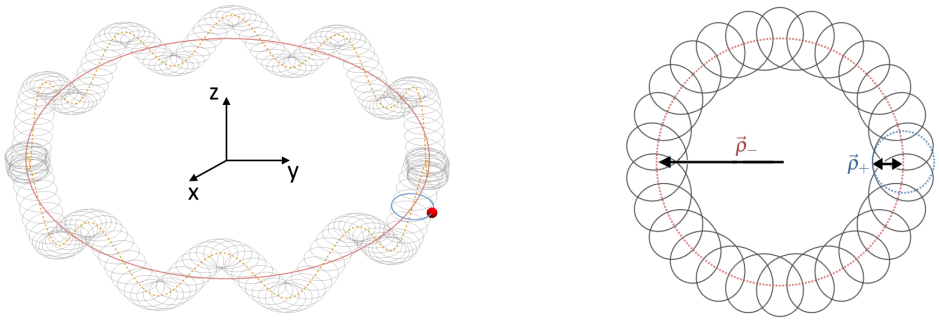

Figure 3: The trajectory of an ion in a Penning trap in 3D (left) and projected on the x-y plane (right). The red curves represent the magnetron motion, and the blue the reduced cyclotron motion. Not drawn to scale.

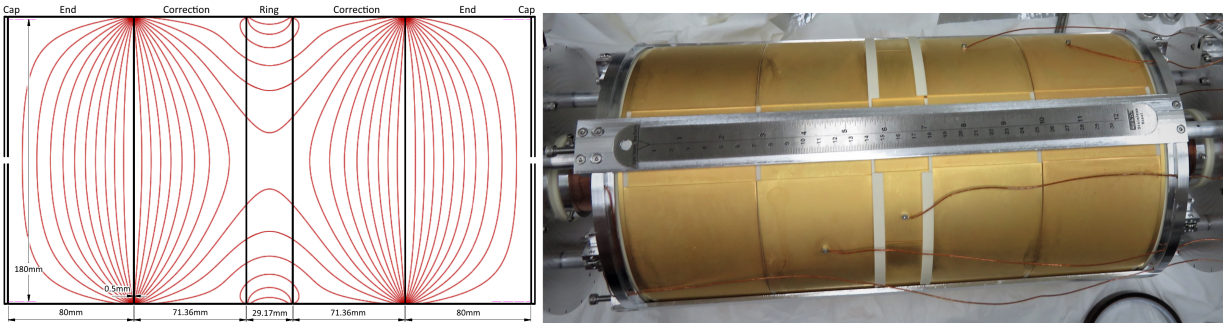

Figure 4: Left: TAMUTRAP's Penning trap electric field lines. These were calculated using SIMION [6, 9]. The ring electrode is segmented into four pieces. Right: The trap with a 12-inch ruler laid on top for scale.

is achieved by alternating neighboring segments, which produces a rolling effect. This couples the magnetron and reduced cyclotron eigenmotions and allows for energy to be transferred between these two planar motions. This quadrupole excitation is the heart of the mass measurements performed with Penning traps and give the time-of-flight (TOF) spectra their iconic structure.

2.2 Time-of-Flight Ion-Cyclotron Resonances

Any precision mass measurement is based on the fact that the cyclotron frequency of an ion in charge state q in a magnetic field B is inversely proportional to its mass:

$$\omega_c = \frac{qB}{m}. \tag{7}$$

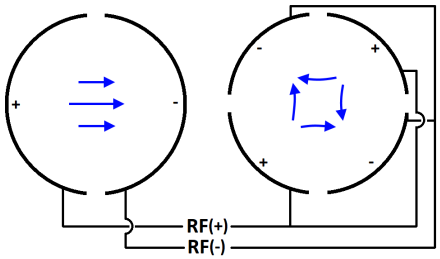

Figure 5: The left electrode/voltage configuration shows dipole excitation. The right shows quadrupole excitation. Note that under oscillations the field arrows continuously flip back and forth.

Since frequencies can be measured very precisely, this provides a powerful manner for determining masses. The basic idea behind the time-of-flight ion-cyclotron resonance (TOF-ICR) technique is as follows [10, 11, 12]. Ions are first cooled in a Penning trap and then their magnetron radius is increased via an applied rf dipole excitation. This motion gives rise to an orbital magnetic moment, μ, which has an associated radial energy $E_r = \mu B$. Once prepared in this state, a quadrupole excitation is applied for a time T_{rf} at a frequency ω_{rf}. With an appropriately chosen amplitude and excitation time and if $\omega_{\text{rf}} = \omega_c$, the quadrpole excitation is in resonance and completely converts the magnetron motion to reduced cyclotron motion. This dramatically increases the radial energy (since $\omega_+ \approx 10^4\,\omega_-$) and hence the magnetic moment of the ion. When released from the trap, the magnetic moment interacts with the magnetic field gradient as it leaves the magnet and is accelerated toward a micro-channel plate (MCP) detector upstream of the trap (as depicted in Fig. 2). The observed time of flight (TOF) will be a minimum when the quadrupole excitation is in resonance with the cyclotron frequency of the ion and the radial energy is a maximum.

To determine the cyclotron frequency of an ion, the measurement described above is performed for different excitation frequencies ω_{rf}. The result is a TOF resonance scan as shown in Fig. 6. This characteristic shape can be understood as arising from the radial energy gained by the ion from the quadrupole excitation [12]:

$$E_r \propto \frac{\sin^2\left(\omega_B T_{\text{rf}}\right)}{\omega_B^2} = \operatorname{sinc}^2(\omega_B T_{\text{rf}}) \tag{8}$$

where

$$\omega_B = \frac{1}{2}\sqrt{\left(\omega_c - \omega_{\text{rf}}\right)^2 + \left(\frac{\pi}{T_{\text{rf}}}\right)^2}. \tag{9}$$

The TOF of the ion from the trap center ($z = 0$) to the MCP detector (at $z = z_{\text{MCP}}$) for a given radial energy may be calculated by

$$T_{\text{TOF}}(\omega) = \int_0^{z_{\text{MCP}}} \sqrt{\frac{m}{2\left[E_0 - qU(z) - \mu(\omega)B(z)\right]}}\,\mathrm{d}z\,, \tag{10}$$

where E_0 is the initial axial energy of the ion, $U(z)$ and $B(z)$ are the electric and magnetic potentials along the ion's trajectory. The sinc function of Eq. (8) leads to the shape of the resonance scan in Fig. 6, but a proper evaluation of the integral requires numerical integration. In order to provide the best fits possible to these TOF resonance scans, the Time Of Flight Fitter and Integrator (TOFFI) program was created to evaluate Eq. (10). The electric potential is taken from outputs of SIMION simulations made specifically with TAMUTRAP's geometries and fields. The magnetic field used is from measurements made during the installation of the super-conducting solenoid magnet. Both are interpolated in order to integrate at any resolution. The integral can be evaluated by either of three methods: Gaussian quadrature rule, trapezoidal rule, and antiderivative through approximation. The latter is done through approximating the kinetic energy via the electric potential and magnetic field as a second order polynomial along the z-axis. TOFFI is used to perform standard χ^2 minimization fits to TAMUTRAP's resonance scans and, as Fig. 6 shows, it provides a very good model of the TOF. The deduced cyclotron frequency of these fit was found not to depend significantly on the integration method used.

2.3 Dampening Effects

As we continued commissioning the facility, we extended the excitation times in order to improve the uncertainty of the fitted resonant frequency. The downside to this is that it allows a greater time for

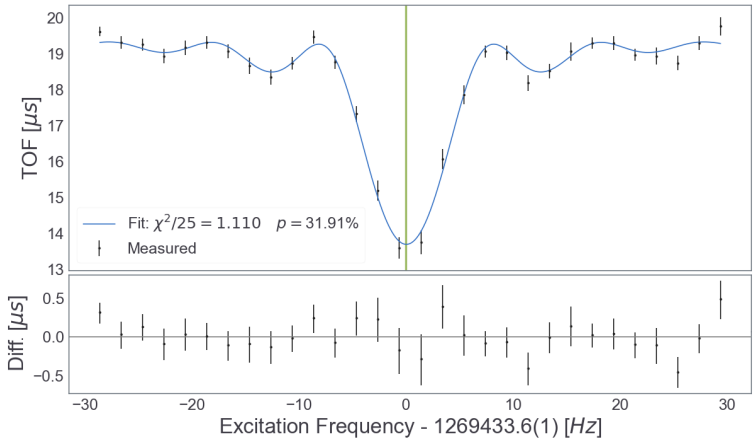

Figure 6: TOF resonance scan for $^{85}\mathrm{Rb}$. The data points are the mean TOF observed in the MCP. The characteristic shape of the spectrum arises from resonant quadrupolar rf excitation, with the minimum at the cyclotron frequency of the ion. The curve is a fit using the program TOFFI.

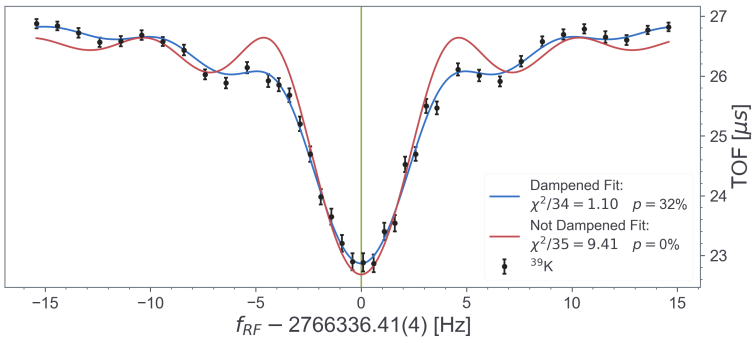

Figure 7: Resonance scan of $^{39}\mathrm{K}^{+}$ with a high pressure of background He gas from the RFQ. Accounting for dampening effects (blue curve) is critical for being able to fit the data. Once included, the quality of the fit dramatically increases compared to ignoring dampening (red curve).

ions in the trap to interact with the background He gas, creating a frictional force on the trapped ions that is no longer negligible, dampening the resonance curve. Figure 7 shows a resonance scan of $^{39}\mathrm{K}^{+}$ taken at the relatively high-pressure of $(3.8 - 4.0) \times 10^{-7}$ mbar. Comparing to Fig. 6, one can clearly see that the sinc-function shape (red curve) is highly attenuated and does not fit the data; dampening effects must be included in order to be able to measure the cyclotron frequency in these cases.

We describe the effect of the background gas on a trapped ion as a viscous force:

$$\vec{F} = -\delta m \vec{v} \tag{11}$$

where the dampening coefficient is

$$\delta \equiv \frac{q}{m} \frac{1}{M_{\mathrm{ion}}} \frac{p/p_{\mathrm{N}}}{T/T_{\mathrm{N}}}. \tag{12}$$

Here M_{ion} is the ion mobility, p is the pressure relative to normal pressure ($p_{\mathrm{N}} = 1013.25$ mbar), and T is the gas temperature relative to normal temperature ($T_{\mathrm{N}} = 300$ K). The effect of the viscous force is to damp the motional amplitudes [13, 11]

$$\rho_{\pm}(t) = \rho_{\pm}(0)\, \exp\left(\mp \gamma \omega_{\pm} t\right) \tag{13}$$

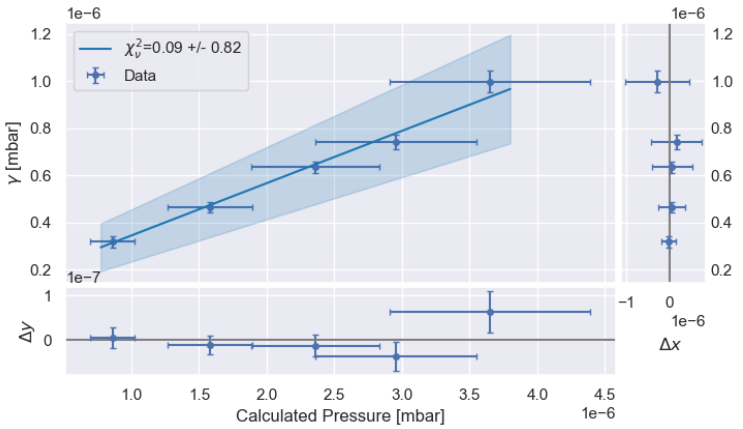

Figure 8: By performing measurements at various trap pressures, we can measure γ as a function of pressure. If the assumed model is correct, a straight line should (and is) produced.

with

$$\gamma = \frac{\delta}{\omega_+ - \omega_-}. \tag{14}$$

Note that for magnetron motion (the lower sign), the amplitude *increases*; this is the key to buffer-gas cooling, where the reduced cyclotron motion is damped and converted to magnetron motion at larger radii.

The effect of dampening was implemented in TOFFI, adding γ as an additional fit parameter. Referring to Fig. 7 again, inclusion of dampening in this way allows us to fit even highly attenuated resonance scans. In order to check that this representation and its implementation is correct, a systematic study was performed. TOF data for $^{39}\mathrm{K}^+$ was taken at varying background gas pressures in the trap by adjusting the helium flow to the RFQ. According to Eqs. (12) and (14), we expect a linear relationship between pressure and the γ returned from the fits. Figure 8 shows the result of this study, and indeed a linear dependence is seen. Unfortunately, it is difficult to definitively determine the pressure at the trap centre; we must interpolate with calculations between two pressure gauges outside of the magnet as shown in Fig. 9. Thus we assign large uncertainties to the pressures in Fig. 8. Qualitatively, the modelling of dampening seems correct, however our fit values for the straight-line fit are not in agreement with expectations: the slope is a factor of 3.6(7) times higher than expected. In future, we plan to better determine the pressure by measuring it from the lifetime of ions in the trap.

3 Commissioning TAMUTRAP

When I started working on this project, TAMUTRAP had recently commissioned its half-scale prototype Penning trap [4]. Since then, many hardware improvements have been implemented, most notably the design and installation of the full-sized Penning trap (Fig. 4) [14]. Operational improvements include software development which allows for the remote and autonomous operation of scans and minimization of systematic errors.

3.1 Optimizing TOF-ICR Curves

Time of Flight Fitter and Integrator (TOFFI) As discussed earlier, TOFFI is used to fit the resonance curves obtained using the TOF-ICR technique. Prior to the establishment of TOFFI, spectra

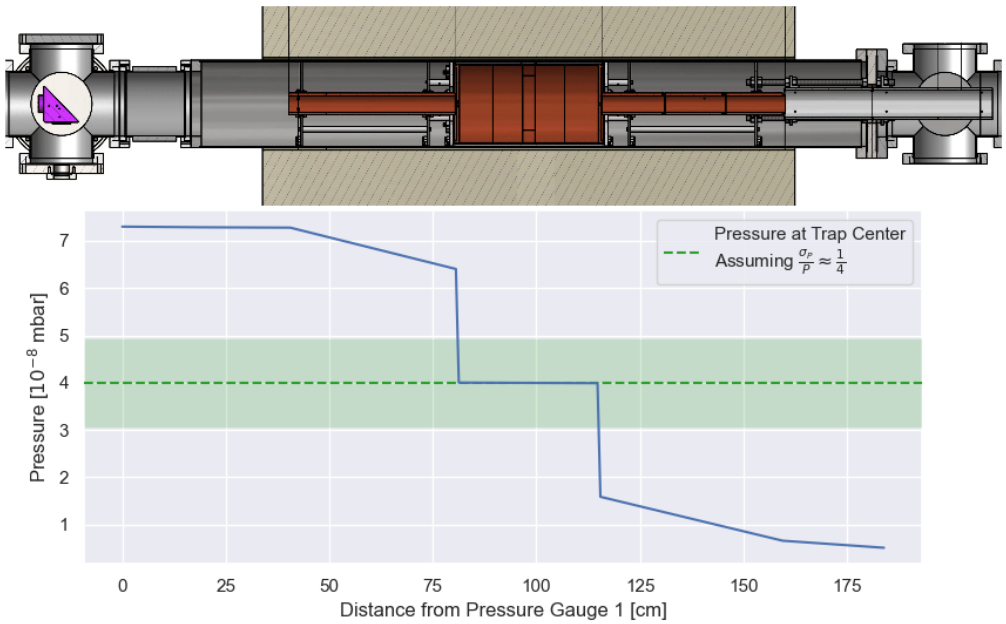

Figure 9: Calculated pressure along the beamline between the two pressure gauges on either side of the super-conducting solenoidal magnet (blue curve). A close-up CAD drawing is shown above the plot as a visual guide. The relatively large steps in pressure are due to the injection and ejection holes of the trap which act as differential pumping apertures. The dashed green line shows the calculated pressure at the trap center, and the green filled area represents the uncertainty dominated by the $\sim \pm 30\%$ accuracy listed in the gauges' operation manual.

at the facility were fit to just the sinc function, which is an approximation of the actual TOF. The TOFFI program not only provides a simpler and more robust interface for analyzing resonance scans, but the numerical integration of Eq. (10) is a much more realistic model for the fitting function. Without the sophisticated analysis of TOFFI, spectra exhibiting dampening effects could not be fit so long excitation times could not be analyzed. The TOFFI program overcomes this limitation and is allowing TAMUTRAP to excite for longer times.

Scan Automation System (SAS) Originally, TOF measurements required the manual adjustment of many power supplies and function generators. Each frequency point on such a curve would take 10–15 mins to complete, and a whole scan a couple of hours. In that time, the magnetic field of the solenoid could drift, introducing an undesired bias to the frequency scan. What was desired was the ability to take many more short (~ 2 mins) runs at a given frequency, and to sweep over the resonance multiple times, not necessarily sequentially; doing this would better average over drifts in the B field and lead to more symmetric resonance curves. Note from Figs. 6 and 7 that our statistical uncertainty in determining the cyclotron frequency is $\lesssim 0.1$ Hz. From Eq. (7), a shift of this magnitude corresponds to a 10^{-6} T change in the field; drifts of a few ppm over the timescale of a day due to, e.g. temperature changes, are expected. When a scan takes a couple of hours, the final field is significantly different from the start, which of course negatively biases the resonance curve.

The Scan Automated System (SAS) program was created to overcome this by automating as much of the scan as possible. It remotely controls the power supplies and function generators, greatly reducing time to perform a scan by minimizing the overhead of manually setting up the equipment. Since implementing SAS, our resonance curves are more reliably symmetric about the cyclotron frequency and result in better χ^2 when fitting. In addition to minimizing this important source of systematics, SAS also lets us run more efficiently and with less user errors.

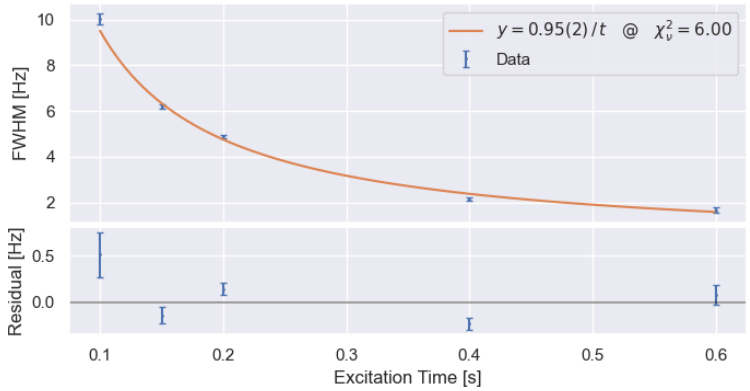

Figure 10: Five FWHM over five different excitation times. For excitation times of 100 ms and 200 ms, there were multiple FWHM which we averaged into single data points following the Particle Data Group (PDG) protocol [19]. This method is to take the points and fit them to a constant with the appropriate statistics, and then use the resulting fitted constant and uncertainty as the new singular point. The confidence for $\chi^2/4 = 6$ here is 20%

Applying quadrupole excitations for longer times For a TOF spectra with no background gas ($\gamma = 0$), the FWHM of a resonance may be estimated by a Taylor expansion of Eq. (8) and is approximately given by [15]

$$\text{FWHM} \approx \frac{0.8}{T_{\text{rf}}}. \tag{15}$$

Clearly, we can improve the precision of our cyclotron frequency measurements by simply exciting for longer times. As mentioned above, however, this gets limited by the finite vacuum and dampening effects which unsurprisingly increases the FWHM the greater γ becomes. Even with dampening, however, the FWHM should still depend inversely with the excitation time. We endeavoured to confirm this by taking resonance curves for varying excitation times. The FWHM of these spectra were evaluated numerically from the fit resonance curve. To estimate the uncertainty in the FWHM (which is not a fit parameter), we used a MC technique to propagate uncertainties: by randomly varying each fit parameter by its uncertainties, we obtained the range of FWHMs consistent with the data. The result of this study is shown in Fig. 10. While it appears we have slightly broader widths compared to the expectation from Eq. (15), a $1/T_{\text{rf}}$ dependence is clearly evident. We suspect that non-negligible dampening effects are the source of the broadening.

The Ramsey method Recently we have started developing another technique for determining the cyclotron frequency to greater precision, known as Ramsey's method of separated oscillatory fields [16, 17]. In this technique, excitation with two Ramsey pulses are applied with a waiting period between them. The Ramsey method promises higher precision through the smaller width of the observed Ramsey fringes compared to the sinc-like function of the regular TOF-ICR technique. SAS and TOFFI were both upgraded to be able to perform these measurements, an example of which is shown in Fig. 11. Note that the FWHM of the Ramsey fringes are $\sim 40\%$ smaller than the regular TOF-ICR curves in Figs. 6 and 7, demonstrating the efficacy of this technique.

3.2 Single-trap Isotopic Mass Separation

Although we differentially pump away much of the helium from the RFQ cooler and buncher, the helium gas from the RFQ does lead to a finite vacuum in the Penning trap. As mentioned earlier, depending

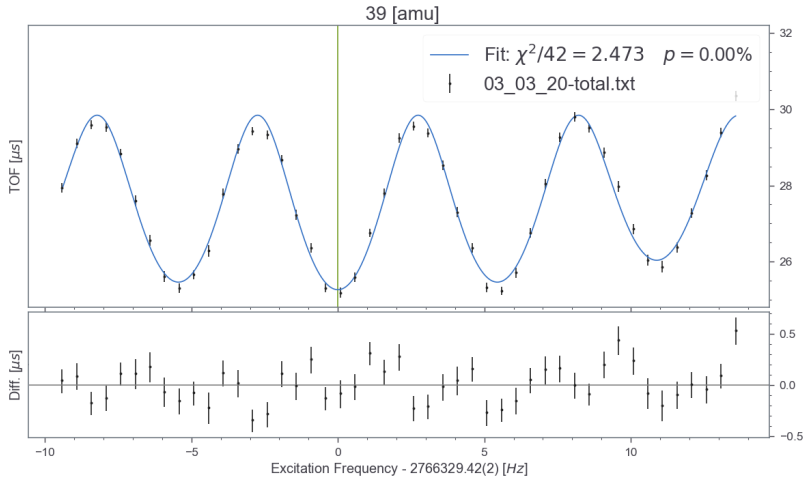

Figure 11: A TOF-ICR resonance curve for $^{39}K^+$ ions obtained with two separate excitation instead of one continuous one (Ramsey's method of time-separated oscillatory fields). An on-off-on excitation pattern of $25 - 150 - 25$ ms was used.

on the pressure we use for cooling and bunching, this leads to unwanted dampening effects. However, this finite vacuum can also be used to our advantage: the background helium gas may be used for purification within our Penning trap.

The process of purification begins with the capturing of the bunched beam of numerous isotopes. The bunch is held momentarily in order to cool the ions to a more stationary state (primarily for dampening axial motion). Next is to apply a mass-independent ω_--dipole excitation to bring all of the ions into a ring radially outwards, past the radius of the extraction hole. Finally, a mass-selective quadrupole excitation is performed at the isotope of interest's cyclotron frequency; this resonant excitation converts the magnetron motion into reduced cyclotron motion only for the ions that have $\omega_{\text{rf}} = \omega_c$. With the magnetron radius greatly reduced for just the ions of interest, these are the only ions which pass through the extraction hole when the bunch is released. The other ions, still at a large magnetron radius, collide with the endcap electrode. In this way, the ions of interest are separated from any other species.

Although many groups already utilize this purification technique, all of them have a dedicated "purification" Penning trap prior to injection in their "measurement" trap. To show the ability to be able to purify a cocktail beam using our single trap, we performed a TOF-ICR measurement using a natural abundance source of rubidium and attempted to use the background He gas to separate ^{87}Rb from ^{85}Rb. A schematic of the timing we used is shown in Fig. 12. Figure 13 shows the resonance curves we obtained when scanning frequencies near both isotopes' cyclotron frequency. The red points show the curves with no purification, and one can see (damped) TOF-ICR curves for both species. Not surprisingly, the minimum for ^{85}Rb is deeper than ^{87}Rb since their natural abundances are 72.17(2)% and 27.83(2)%, respectively. The black points show the same TOF-ICR spectra following purification. The clear dip in the ^{87}Rb curve without purification becomes almost consistent with zero following purification, while the resonance for ^{85}Rb gets a little more pronounced. Upon fitting TOF-ICR curves to these data, the amplitude for ^{85}Rb increases from $4.3(4)$ μs before purification to $5.2(3)$ μs following purification. This increase makes sense because with less ^{87}Rb contaminating the TOF spectrum, the resonance curve should be more pronounced. Conversely, looking at the ^{87}Rb data we see the amplitude goes from $2.3(2)$ μs down to $0.6(4)$ μs following purification; the 1.5σ 'signal' after purification is roughly consistent with zero.

Qualitatively, it is clear that the single-trap purification scheme is working. This is, as far as we are aware, the first time a single Penning trap has been used for purification *and* measuring the cyclotron

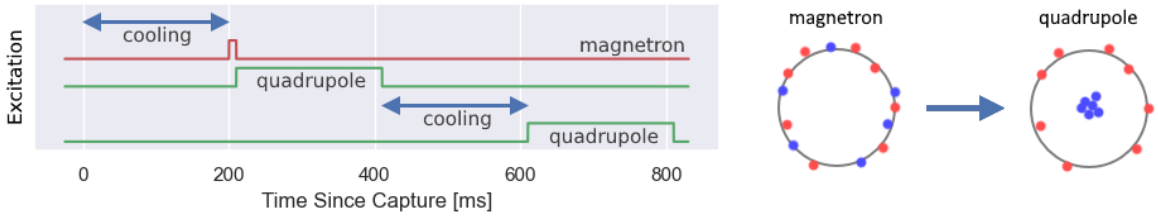

Figure 12: Left: timing diagram of the rf excitations for purification. We start with 200 ms of cooling the ions and preparing them for the magnetron excitation to move both species, wanted (blue) and unwanted (red), to a larger radius. We then apply a quadrupole pulse to selectively bring the ions of interest (blue circles) back to the trap center. We then cool the ions again before applying a 2nd quadrupole excitation for the TOF-ICR measurement.

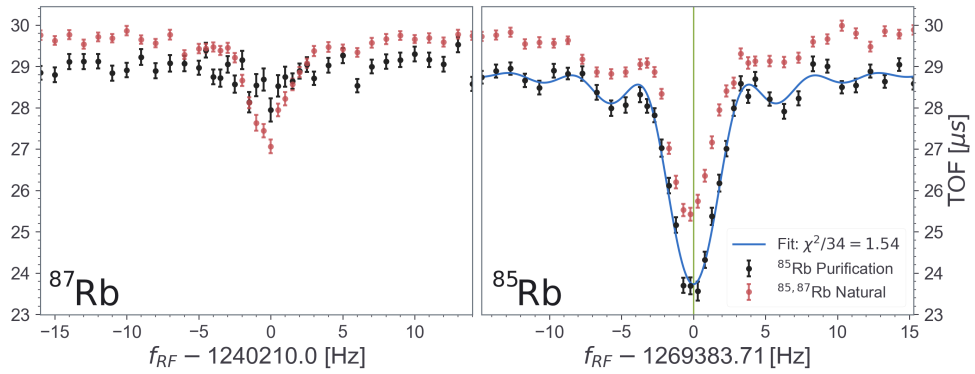

Figure 13: TOF data taken with (black) and without (red) the isotopic mass separation (removal) of $^{87}\mathrm{Rb}^{+}$. The left panel shows the TOF curve over frequencies relevant for $^{87}\mathrm{Rb}^{+}$, and the right spans frequencies near ω_c for $^{85}\mathrm{Rb}^{+}$.

frequency. The goal of this measurement was to demonstrate the ability to purify ions in TAMUTRAP, and we have succeeded. This will not be a part of the β-delayed proton decay program since those decays are so distinctive and short-lived, backgrounds will not compromise decay measurements. However, if we (or any other group at the CI) desire an ultra-pure, low-energy beam of isotopes from TAMUTRAP, this purification scheme can be used to provide it.

3.3 Mass Measurements of Stable Alkali

In theory, one can measure the mass directly from the the resonant frequency found in the TOF through the cyclotron frequency $\omega_c = qB/m$. The field however must be known extremely well, $\lesssim 10^{-6}$ T as mentioned earlier. In order to avoid needing to measure the field so precisely, the solution is to compare the measured cyclotron frequency to that of a reference ion of known mass, *i.e.* as tabulated in the Atomic Mass Evaluation (AME) [18]. For two singly-charged ions with neutral *atomic* masses m and m_{ref}, their ratio of cyclotron frequencies from Eq. (7) will be

$$\frac{\omega_c}{\omega_c^{\mathrm{ref}}} = \left(\frac{B}{B_{\mathrm{ref}}}\right)\left(\frac{m_{\mathrm{ref}} - m_e}{m - m_e}\right), \tag{16}$$

where the subtraction of electron masses is because the are singly-charged ions. This relation can be rearranged to give

$$m = \left(\frac{\omega_c^{\mathrm{ref}}}{\omega_c}\right)(m_{\mathrm{ref}} - m_e) + m_e \tag{17}$$

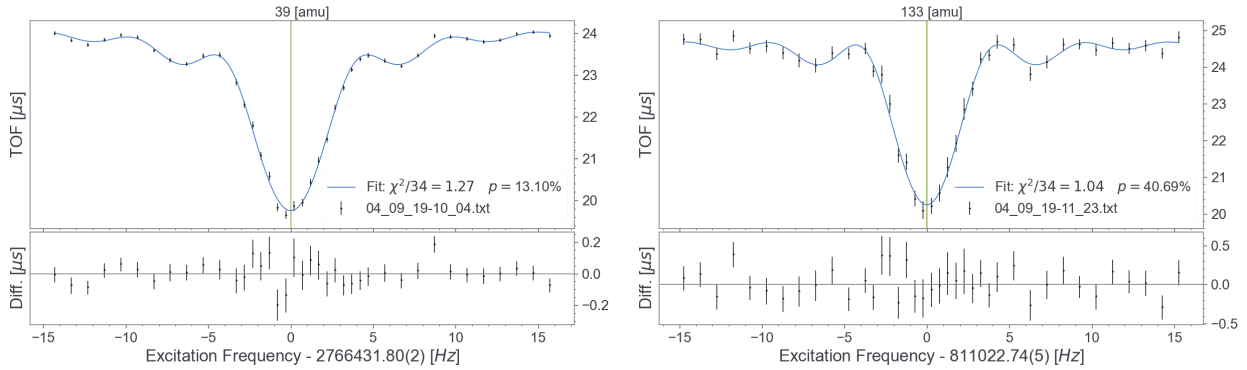

Figure 14: Resonance spectra for $^{39}\mathrm{K}^{+}$ and $^{133}\mathrm{Cs}^{+}$ are shown on the left and right respectively. The two were measured sequentially, so the magnetic field between the two should have minimal deviation. $^{39}\mathrm{K}^{+}$ is the reference for measuring the mass of $^{133}\mathrm{Cs}^{+}$.

where we assume that $B \approx B_{\mathrm{ref}}$ which is reasonable if the second cyclotron frequency is measured immediately following the first. The electron mass accounts for the fact that we have an ion in the trap rather than a neutral atom.

In commissioning TAMUTRAP with offline mass measurements, we always try to take $^{39}\mathrm{K}$ as the reference mass. For measurements of $^{23}\mathrm{Na}$ and $^{133}\mathrm{Cs}$, $^{39}\mathrm{K}$ was used as the reference, whereas for $^{87}\mathrm{Rb}$ the reference was $^{85}\mathrm{Rb}$. Of course all of these masses are already very well known; we performed these mass measurements to gain experience manipulating trapped ions, to optimize the efficiency of the system, and to prove we can perform mass measurements which are not biased and which agree with the literature values [18].

For each mass measurement, a TOF-ICR resonance curve was generated for the species of interest using SAS back-to-back with the reference ion. The cyclotron frequencies were fit using TOFFI and then Eq. (17) was used to deduce the atom's mass. An example of two such resonance curves and their fits are shown in Fig. 14. The deduced mass for $^{133}\mathrm{Cs}$ is 132.905 477(8) amu which is 3σ larger than the accepted value [18] of 132.905 451 961(8) amu. This is one of a number of measurements of $^{133}\mathrm{Cs}$, which are all summarized graphically in the right panel of Fig. 15. The average of the 6 measurements shows a small bias with a difference from the AME of -7.4 ± 5.2 keV (1.5σ). The source of the systematic shift to larger values for this isotope needs to be investigated; nevertheless, the statistical uncertainty leads to a mass resolution of $\Delta M/M = 42$ parts-per-billion (ppb). The other two lighter alkalis studied, $^{23}\mathrm{Na}$ and $^{87}\mathrm{Rb}$, are in good agreement with the literature values, showing mass resolutions of 21 and 36 ppb.

As discussed earlier, we have investigated different durations of rf excitation, from $100-600$ ms. The times for each measurement is indicated in Fig. 15. In general, the uncertainties are smaller for longer excitation times, most dramatically for the 200 ms $^{23}\mathrm{Na}$ compared to 100 ms. The reason this is not consistently true (see, for example, the two $^{87}\mathrm{Rb}$ points with 200 ms excitation) is because uncertainties from the fit are all multiplied by the $\sqrt{\chi^2/\mathrm{dof}}$ if the fit is poor [19]. The cyclotron frequencies for all of the mass measurements shown in Fig. 15 are listed in the appendix, Table A2.

The ability to measure masses to precisions of $\lesssim 50$ ppb demonstrates our novel large-diameter Penning trap — by far the world's largest — operates as expected. This level of precision is on par with other labs using the TOF-ICR technique (albeit on short-lived radioactive ions). Based on these results, the TAMUTRAP facility with the unique 180-mm cylindrical Penning trap is considered commissioned. It is worth pointing out that ultra-precise mass measurements is not the goal of TAMUTRAP, though if we find a case where the mass could be improved, we are ready to perform such measurements.

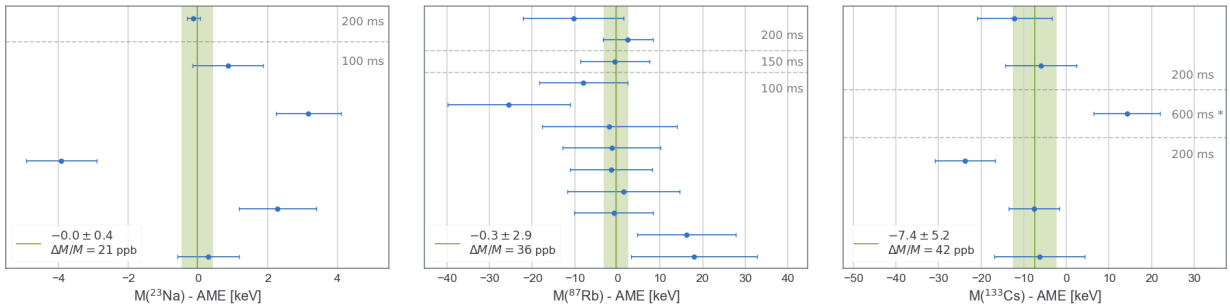

Figure 15: Mass measurements of ^{23}Na, ^{87}Rb, and ^{133}Cs. The reference ions for ^{23}Na and ^{133}Cs were ^{39}K. The reference ion for ^{87}Rb was ^{85}Rb. The relative uncertainties are listed in the legends of the plots. The dashed lines and times shown in gray indicate the regions where excitation times differ. Each point comes from a pair of TOF measurements. The excitation times are the same for both isotopes in a given pair. The "600 ms*" excitation in the right plot had a mixed set of excitation times, 600 ms for ^{133}Cs and 200 ms for ^{39}K.

4 Conclusions and Future Directions

The β-delayed proton decay studies planned with TAMUTRAP requires a unique Penning trap with a length-to-radius ratio that is $3.2\times$ smaller than typical cylindrical Penning traps. This report describes its commissioning through performing mass measurements using the TOF-ICR technique to $\lesssim 50$ ppb, comparable to the typical traps used at other facilities. Tools have been developed to perform (SAS) and analyze (TOFFI) these measurements, whether dampening effects are present or not. Optimization of TAMUTRAP, which is very important given the low rates of RIBs expected of the very neutron-deficient nuclei to be studied, is proceeding. In addition, improvements to the TOF-ICR technique as well as implementing the Ramsey method for enhanced precision in mass measurements are ongoing.

One of the efforts we will be pursuing next is reduction of the background helium gas from the RFQ so as to allow us to utilize longer excitation times and improve the precision of our mass-measurements. For this we plan to add additional vacuum pumps and perhaps add more differential-pumping apertures between the RFQ and trap. In parallel, we will continue to develop TOFFI and perform a more systematic study of the dampening effects of the He gas. By sampling more trap pressures and optimizing the excitation time for each pressure setting, we will be able to extend our range of dampening parameters; although the general dependence of γ on pressure was found to be linear, we would like to obtain quantitative agreement with the expected slope of Fig. 8.

We have only just started measuring cyclotron frequencies using the Ramsey excitation scheme, and will soon switch to using it for the improved precision it offers. This is especially important if/when we do measure masses of short-lived radioactive ions once RIB is transported to TAMUTRAP: the lifetime of the ion may limit the resolution possible from the regular TOF-ICR, while the Ramsey approach can reach the same precision with a shorter measurement cycle. In particular, after we re-establish the working order of the TAMUTRAP facility following the shutdown from covid-19 and develop TOFFI/SAS a little more, we are planning a comprehensive campaign of measuring masses of ^{23}Na, ^{41}K, ^{85,87}Rb and ^{133}Cs (using ^{39}K as the reference mass). We will publish these results in Phys. Rev. Accels. and Beams, the Int. J. Mass Spec. or NIMA, concentrating on the dampening effects study as the literature is relatively sparse on this topic.

A Mass Measurement Values and Details

Table A1 show the values taken from the 2017 AME [18]. They are the values used in mass measurement calculations. The software created to perform these calculations pulls these values directly from AME's online resource, ensuring the latest values are are always used. Table A2 shows the data used for the mass differences shown in Fig. 15. The excitation times are reported along with the resonant frequencies as to help clarify varying uncertainties.

Table A1: Atomic masses from the AME used by TAMUTRAP software. Values for the electron mass and conversion of atomic mass units to keV are taken from the 2018 recommended values from the Committee on Data for Science and Technology (CODATA) [20]: $m_e = 510.998\,946(3)$ keV and 1 amu $= 931\,494.095(6)$ keV.

Isotope	Atomic Mass [amu]	Mass Excess [keV]
^{23}Na	22.989 769 282(2)	-9 529.852(2)
^{39}K	38.963 706 487(5)	-33 807.190(5)
^{85}Rb	84.911 789 738(5)	-82 167.331(5)
^{87}Rb	86.909 180 531(6)	-84 597.791(6)
^{133}Cs	132.905 451 961(8)	-88 070.931(8)

Table A2: Pairs of nuclides for which resonance scans were performed for mass measurements. Listed are the cyclotron frequencies from the fit, f_c (in Hz), as well as the quadrupole excitation time, T_{rf} (in ms). The lower isotope of each pair is the reference ion for measuring the mass of the upper isotope.

Isotope	f_c	T_{rf}
^{23}Na$^+$	4688671.86(11)	100
^{39}K$^+$	2766431.58(9)	100
^{23}Na$^+$	4688684.98(14)	100
^{39}K$^+$	2766439.07(12)	100
^{23}Na$^+$	4688684.84(14)	100
^{39}K$^+$	2766439.79(10)	100
^{23}Na$^+$	4688683.31(14)	100
^{39}K$^+$	2766437.97(9)	100
^{23}Na$^+$	4688670.28(15)	100
^{39}K$^+$	2766430.58(10)	100
^{23}Na$^+$	4688672.17(2)	200
^{39}K$^+$	2766431.82(2)	200
^{87}Rb$^+$	1240255.22(21)	100
^{85}Rb$^+$	1269429.81(8)	100
^{87}Rb$^+$	1240255.08(15)	100
^{85}Rb$^+$	1269429.69(10)	100

Isotope	f_c	T_{rf}
^{87}Rb$^+$	1240254.94(9)	100
^{85}Rb$^+$	1269429.81(11)	100
^{87}Rb$^+$	1240254.80(11)	100
^{85}Rb$^+$	1269429.63(17)	100
^{87}Rb$^+$	1240254.80(11)	100
^{85}Rb$^+$	1269429.68(10)	100
^{87}Rb$^+$	1240254.80(15)	100
^{85}Rb$^+$	1269429.68(10)	100
^{87}Rb$^+$	1240254.86(20)	100
^{85}Rb$^+$	1269429.75(14)	100
^{87}Rb$^+$	1240255.75(18)	100
^{85}Rb$^+$	1269431.03(12)	100
^{87}Rb$^+$	1240255.94(13)	100
^{85}Rb$^+$	1269430.95(9)	100
^{87}Rb$^+$	1240256.15(10)	150
^{85}Rb$^+$	1269431.05(7)	150

Isotope	f_c	T_{rf}
^{87}Rb$^+$	1240256.01(5)	200
^{85}Rb$^+$	1269430.86(7)	200
^{87}Rb$^+$	1240256.01(5)	200
^{85}Rb$^+$	1269431.06(18)	200
^{133}Cs$^+$	811021.54(7)	200
^{39}K$^+$	2766427.34(2)	200
^{133}Cs$^+$	811025.46(4)	200
^{39}K$^+$	2766440.74(5)	200
^{133}Cs$^+$	811022.74(5)	200
^{39}K$^+$	2766431.80(2)	200
^{133}Cs$^+$	811023.09(5)	600
^{39}K$^+$	2766432.17(7)	200
^{133}Cs$^+$	811022.98(5)	200
^{39}K$^+$	2766432.22(3)	200
^{133}Cs$^+$	811022.88(6)	200
^{39}K$^+$	2766432.05(3)	200

References

[1] M. Mehlman, P. Shidling, S. Behling, L. Clark, B. Fenker, D. Melconian, Design of a unique open-geometry cylindrical Penning trap, Nucl. Instrum. and Methods Phys. Res. A **712**, 9 (2013).

[2] J. Jackson, S. Trieman, H. Wyld, Coulomb corrections in allowed beta transitions, Nucl. Phys. A **4**, 206 (1957).

[3] J.D. Jackson, S.B. Trieman, H.W. Wyld, Possible tests of time reversal invariance in beta decay, Phys. Rev. **106**, 517 (1957).

[4] P. Shidling, V. Kolhinen, B. Schroeder, M. Nasser, A. Ozmetin, D. Melconian, TAMUTRAP facility: Penning trap facility for weak interaction studies, Hyperfine Interact. **240**, 40 (2019).

[5] W. Paul, Electromagnetic traps for charged and neutral particles, Rev. Mod. Phys. **62**, 531–540 (1990).

[6] M. Mehlman, Development of the TAMUTRAP facility for precision beta-decay studies, Ph.D. thesis, Texas A&M University (2015).

[7] P. Shidling, V. Kolhinen, B. Schroeder, M. Nasser, A. Ozmetin, D. Melconian, Ion-trap application: Fundamental weak interaction studies using ion traps, AIP Conference Proceedings **2160**, 070011 (2019).

[8] H. Raimbault-Hartmann, D. Beck, G. Bollen, M. König, H.-J. Kluge, E. Schark, J. Stein, S. Schwarz, J. Szerypo, A cylindrical Penning trap for capture, mass selective cooling, and bunching of radioactive ion beams, Nucl. Instrum. and Methods Phys. Res. B **126**, 378 (1997).

[9] Scientific Instrument Services Inc., SIMION 8.1 (2012), http://simion.com.

[10] G. Gräff, H. Kalinowsky, J. Traut, A direct determination of the proton electron mass ratio, Z. Phys. A **297**, 35 (1980).

[11] K. Blaum, High-accuracy mass spectrometry with stored ions, Phys. Rep. **425**, 1 (2006).

[12] M. König, G. Bollen, H.-J. Kluge, T. Otto, J. Szerypo, Quadrupole excitation of stored ion motion at the true cyclotron frequency, Int. J. Mass Spec. and Ion Proc. **142**, 95 (1995).

[13] G. Bollen, Traps for rare isotopes, The Euroschool Lectures on Physics with Exotic Beams **651**, 169–210 (2004).

[14] V. Kolhinen, V. Iacob, D. McClain, D. Melconian, M. Nasser, A. Ozmetin, B. Schroeder, P. Shidling, Making the world's largest Penning trap 2× bigger for beta-delayed proton decay studies, Tech. report, Cyclotron Institute, Texas A&M University (2019).

[15] M. König, Präzisionsmassenbestimmung instabiler Cäsium- und Bariumisotope in einer Penningfalle und Untersuchung der Ionenbewegung bei azimuthaler Quadrupolanregung, Ph.D. thesis, Johannes Gutenberg-Universität (1995).

[16] G. Bollen, H.-J. Kluge, T. Otto, G. Savard, H. Stolzenberg, Ramsey technique applied in a Penning trap mass spectrometer, Nucl. Instrum. and Methods Phys. Res. B **70**, 490 (1992).

[17] S. George, S. Baruah, B. Blank, K. Blaum, M. Breitenfeldt, U. Hager, F. Herfurth, A. Herlert, A. Kellerbauer, H.-J. Kluge, M. Kretzschmar, D. Lunney, R. Savreux, S. Schwarz, L. Schweikhard, C. Yazidjian, Ramsey method of separated oscillatory fields for high-precision Penning trap mass spectrometry, Phys. Rev. Lett. **98**, 162501 (2007).

[18] M. Wang, G. Audi, F. G. Kondev, W. Huang, S. Naimi, X. Xu, The AME2016 atomic mass evaluation (II). Tables, graphs and references, Chinese Physics C **41** (3), 030003 (2017).

[19] M. Tanabashi, et al., Review of Particle Physics, Phys. Rev. D **98** (3), 030001 (2018), The Particle Data Group.

[20] P. Mohr, D. Newell, B. Taylor, E. Tiesinga (2018), NIST Data Center https://physics.nist.gov/cuu/Constants/index.html.